



**Brownian simulations for tetra-gel-type phantom networks  
composed of prepolymers with bidisperse arm length**

Journal:	<i>Soft Matter</i>
Manuscript ID	SM-ART-04-2022-000488.R1
Article Type:	Paper
Date Submitted by the Author:	14-May-2022
Complete List of Authors:	Masubuchi, Yuichi; Nagoya University, Department of Materials Physics Yamazaki, Ryohei; Nagoya Daigaku Doi, Yuya; Nagoya University, Department of Materials Physics Uneyama, Takashi; Nagoya University, Department of Materials Physics Sakumichi, Naoyuki; The University of Tokyo, Graduate School of Engineering, Depart of Materials Engineering Sakai, Takamasa; The University of Tokyo, Graduate School of Engineering, Depart of Materials Engineering

1 Brownian simulations for tetra-gel-type phantom networks composed of prepolymers with  
2 bidisperse arm length

3  
4 \*<sup>1</sup>Yuichi Masubuchi, <sup>2</sup>Ryohei Yamazaki, <sup>1</sup>Yuya Doi, <sup>1</sup>Takashi Uneyama,  
5 <sup>3</sup>Naoyuki Sakumichi and <sup>3</sup>Takamasa Sakai

6  
7 <sup>1</sup>Department of Materials Physics & <sup>2</sup>Department of Engineering Physics,  
8 Nagoya University, Nagoya 4648603, JAPAN

9 <sup>3</sup>Department of Bioengineering,  
10 The University of Tokyo, Tokyo 1138654, JAPAN

11  
12 \*to whom correspondence should be addressed

13 [mas@mp.pse.nagoya-u.ac.jp](mailto:mas@mp.pse.nagoya-u.ac.jp)

14 TEL: +81-527892551

15  
16 Submitted to Soft Matter

17  
18  
19 **Abstract**

20 We studied the effect of arm length contrast of prepolymers on mechanical properties of  
21 tetra-branched networks via Brownian dynamics simulations. We employed a bead-spring model  
22 without excluded volume interactions, and we did not consider the solvent explicitly. Each examined  
23 4-arm star branch prepolymer has uneven arm lengths to attain two-against-two (2a2) or  
24 one-against-three (1a3) configurations. The arm length contrast was varied from 38-2 to 20-20 for  
25 2a2, and from 5-25 to 65-5 for 1a3, with the fixed total bead number of 81, including the single bead  
26 located at the branch point for prepolymers. We distributed 400 molecules in the simulation box  
27 with periodic boundary conditions, and the bead number density was fixed at 4. We created polymer  
28 networks by cross-end-coupling of equilibrated tetra-branched prepolymers. To mimic the  
29 experiments of tetra gels, we discriminated the molecules into two types and allowed the reaction  
30 only between different types of molecules at their end beads. The final conversion ratio was more  
31 than 99%, at which unreacted dangling ends are negligible. We found that the fraction of double  
32 linkage, two of the four arms connecting a pair of branch points, increases from 3% to 15% by  
33 increasing the arm length contrast. We stretched the resultant tetra-type networks to obtain the ratio  
34 of mechanically effective strands. We found that the ratio is 96% for the monodisperse system,  
35 decreasing to 90% for high arm length contrast. We introduced bond scission according to the bond  
36 stretch to see network fracture under sufficiently slow elongation. The fracture behavior was not

37 correlated to the fraction of double linkage because the scission occurs at single linkages.

38

39 **Keywords:** polymer dynamics, molecular simulations, viscoelasticity

40

## 41 1. INTRODUCTION

42 Tetra gels are known as a class of defect-free polymer networks<sup>1,2</sup>. Wallace et al.<sup>3</sup> first synthesized a  
43 tetra-branched gel created from mixtures of tetra-N-succinimidyl poly (ethylene glycol)  
44 (tetra-NHS-PEG) and tetra-thiol-derivatized PEG (tetra-TD-PEG) for biomedical use. Sakai et al.<sup>4</sup>  
45 employed tetra-amine-derivatized PEG (tetra-AD-PEG) instead of tetra-TD-PEG and defined tetra  
46 gels as polymer gels formed from two tetra-branched prepolymers with mutually reactive functional  
47 groups. They examined the mechanical properties and the network structure of a series of tetra gels.  
48 They found that tetra gels have a uniform network with a negligible number of defects to exhibit  
49 superior mechanical toughness. Here, the defects mean entanglements, loops, unreacted dangling  
50 ends, and polydispersity in the strand length. Due to the binary nature, given that the gelation time is  
51 appropriately tuned, there is no primary loop formation in tetra gels and a limited number of  
52 unreacted ends<sup>5-8</sup>. Besides, one can control the uniformity of the strand length and entanglement  
53 formation by the molecular weight of prepolymers<sup>9,10</sup>. The network uniformity is a distinguishable  
54 feature of tetra gels from the other network polymers, and the studies based on the uniformity have  
55 been made both toward fundamental and application directions<sup>11-15</sup>.

56

57 An interesting approach is to utilize tetra gels as reference materials for studying the effects of  
58 defects. Sakai et al.<sup>16</sup> have conducted such an attempt using tetra gels made of prepolymers with the  
59 arm length contrast. They mixed a monodisperse tetra-NHS-PEG (arm molecular weight of 5k) with  
60 bidisperse tetra-AD-PEGs (arm molecular weights of 1.3k and 5k). The mixtures realize a contrast in  
61 the strand molecular weights of 6.3:10 at the maximum. They have summarized that the examined  
62 arm length contrast does not significantly affect the toughness of resultant gels. We note that if  
63 further contrast is introduced, the inhomogeneous stretch of strands probably depresses the  
64 toughness, as suggested by earlier studies for end-linked<sup>17,18</sup> and randomly cross-linked<sup>19</sup> poly  
65 (dimethylsiloxane) (PDMS) elastomers.

66

67 Although most studies have reported that the inclusion of defects suppresses the mechanical  
68 properties of polymer networks, a few studies imply that some inhomogeneity may improve the  
69 toughness. For instance, Lin and Zhao<sup>20</sup> have theoretically proposed that the fracture energy of  
70 polymer networks increases with increasing the number of double linkages (i.e., cyclic loops in their  
71 terminology). Here, the double linkage expresses connectivity between a pair of network nodes that  
72 share two strands. They calculated the fracture energy from the required work to elongate the strand

73 up to its scission, assuming that double linkages are located on the crack path. The obtained fracture  
74 energy linearly increases with increasing the fraction of double linkages. Although the crack path  
75 may not propagate by selectively cutting double linkages, this direction is worth investigating. For  
76 instance, let us consider an asymmetric tetra-branched polymer having long and short arms as a  
77 prepolymer. In this case, the fraction of double linkages in the resultant gel increases with increasing  
78 the ratio between the molecular weights of long and short arms, as expected from the conformational  
79 distribution function<sup>21</sup>. (We do not consider the primal loop formation, in which two arms of a single  
80 polymer connect because the primal loop is forbidden in the reaction.) Based on the theory, the  
81 toughness of such networks may be better than that of the network made of symmetric prepolymers.  
82 One may argue that this thought contradicts the results by Sakai et al.<sup>16</sup> mentioned above. However,  
83 their range of molecular weight contrast is rather limited, and they only examined the mixtures of  
84 symmetric prepolymers.

85

86 Molecular simulations would be useful for the problem. There have been several simulation studies  
87 for tetra-gel-type networks. Lange et al.<sup>22</sup> have investigated the fraction of double and higher-order  
88 linkages with respect to the prepolymer concentration via a bond-fluctuation Monte Carlo method to  
89 report that the results are qualitatively consistent with NMR measurements. Lin et al.<sup>23</sup> have  
90 performed a similar analysis based on kinetic graph theory in addition to the Monte Carlo  
91 simulations. Nishi et al.<sup>24</sup> have calculated the elastic modulus of a series of tetra-gel-type networks  
92 with varying the connectivity ratio between the network nodes. Sugimura et al.<sup>25</sup> have extended the  
93 method to discuss the fracture. Wang and Escobedo<sup>26</sup> have constructed coarse-grained models of  
94 defect-free tetra-PEG networks to exhibit stress-strain relations. Furuya and Koga<sup>27</sup> performed  
95 bead-spring simulations to see the number of effective strands in the tetra-gel-type networks. Apart  
96 from the simulations for tetra-gel-type networks, very recently, Arora et al.<sup>28</sup> have conducted  
97 simulations for polymer networks made of linear prepolymers and tetra-functional cross-linkers.  
98 They reported that the toughness decreases with increasing the number of primary loops.  
99 Nevertheless, these earlier studies did not discuss the effect of double linkages on mechanical  
100 properties.

101

102 In this study, we performed Brownian dynamics simulations of tetra gel-type networks formed from  
103 prepolymers, for which the arm molecular weight is bidisperse. From such prepolymers, networks  
104 were created via Brownian simulations of gelation. The introduced bidispersity of the arm molecular  
105 weights does not affect the gelation kinetics and the conversion ratio. In contrast, the number of  
106 double linkages increases with increasing the arm length contrast. The resultant networks were  
107 uniaxially stretched, and the number of mechanically effective strands was estimated from the elastic  
108 modulus. We also examined the fracture behavior by introducing bond scission according to the

109 bond stretch to discuss the toughness. The results imply that the inclusion of double linkages does  
 110 not improve the mechanical properties. Details are shown below.

111

## 112 2. MODEL AND SIMULATIONS

113 We consider 4-arm star prepolymers represented by bead-spring chains. All the chains are phantom  
 114 since we neglect the effects of excluded volume interactions, including entanglements. No solvent is  
 115 considered explicitly. The bead position  $\{\mathbf{R}_i\}$  obeys the standard Langevin equation of motion  
 116 written as

$$117 \quad \mathbf{0} = -\zeta \dot{\mathbf{R}}_i + \frac{3k_B T}{a^2} \sum_k f_{ik} \mathbf{b}_{ik} + \mathbf{F}_i$$

118 In RHS, the first term is the drag force, the second term is the contribution of connected springs, and  
 119 the third term is the thermal random force.  $\zeta$  is the friction coefficient,  $a$  is the average bond  
 120 length, and  $\mathbf{b}_{ik} \equiv \mathbf{R}_i - \mathbf{R}_k$  is the bond vector between the connected beads.  $f_{ik}$  is the spring factor  
 121 for finite chain extensibility. We had  $f_{ik} = 1$  for the simulations with Gaussian springs, whereas  
 122  $f_{ik} = (1 - \mathbf{b}_{ik}^2/b_{\max}^2)^{-1}$  with  $b_{\max} = 3$  for the case with the finite extensibility. We have  
 123 confirmed that this choice of  $b_{\max}$  avoids thermal degradation for the examined networks.  $\mathbf{F}_i$  is the  
 124 Gaussian random force, which obeys  $\langle \mathbf{F}_i \rangle = \mathbf{0}$  and  $\langle \mathbf{F}_i(t) \mathbf{F}_j(t') \rangle = 2k_B T \delta_{ij} \delta(t - t') \mathbf{I} / \zeta$ , where  $\mathbf{I}$   
 125 is the unit tensor. We chose units of length, energy, and time as  $a$ ,  $k_B T$  and  $\tau = \zeta a^2 / k_B T$ , and  
 126 quantities reported hereafter are normalized. For the numerical integration, a second-order scheme<sup>29</sup>  
 127 was employed.

128

129 We examined several star prepolymers, as shown in Table I and Figure 1. The arm molecular  
 130 weights were bidispersed in two-against-two (2a2) and one-against-three (1a3) manners. The total  
 131 molecular weight of polymers was fixed at 81, including one bead at the branch point and the other  
 132 80 beads on the stemming arms. We mimicked the formation of tetra gels by considering two types  
 133 of molecules (A and B) that react only with the other type of molecules. The prepolymer  
 134 configurations were common for A and B prepolymers. For comparison, a network created by  
 135 random linking of a single long chain (for which the molecular weight is 32,400) across periodic  
 136 boundary conditions was also provided and subjected to mechanical tests. The number of cross-links  
 137 for this case was common with the tetra systems, and the distribution of the strand length between  
 138 crosslinks is given in Supporting Information.

139

140

**Table I** Examined systems

Code	$N_l^*$	$M_l^{**}$	$N_s^+$	$M_s^{++}$
2a2-3802	38	2	2	2
2a2-3604	36	2	4	2
2a2-3208	32	2	8	2
2a2-2713	27	2	13	2

s2020	20	4	-	-
1a3-0525	25	3	5	1
1a3-1123	23	3	11	1
1a3-3515	35	1	15	3
1a3-5010	50	1	10	3
1a3-6505	65	1	5	3
Rnd#	-	-	-	-

141

\*Number of beads for the long arm.

142

\*\*Number of long arms stemming from the branch point.

143

+Number of beads for the short arm.

144

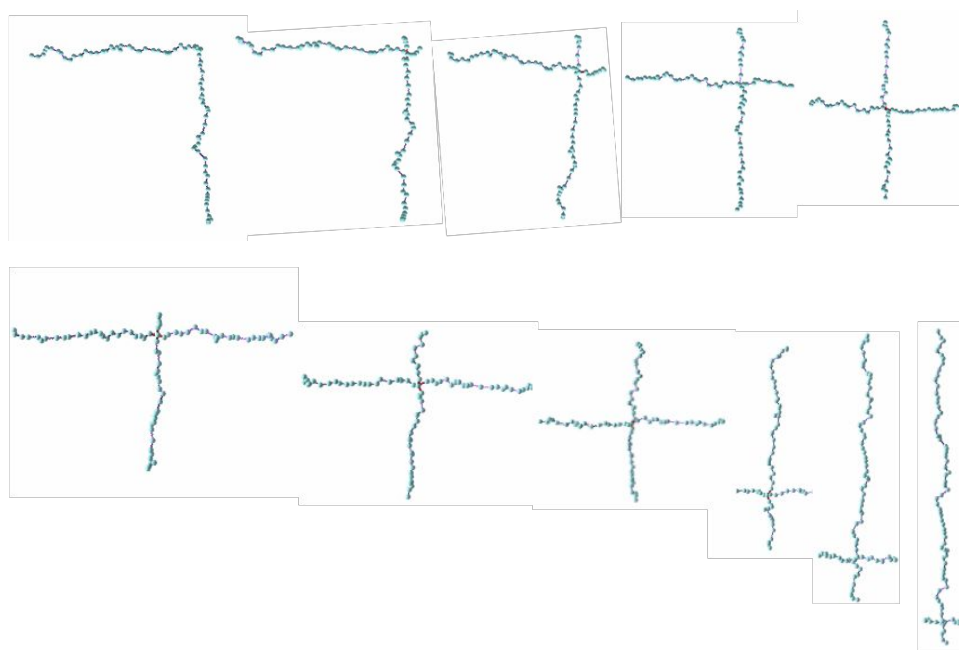
++Number of short arms stemming from the branch point.

145

#Created via random linking of a single long chain

146

147



148

149 **Figure 1** Examined two-against-two (top) and one-against-three (bottom) type prepolymers. The  
 150 sample codes from left to right are 2a2-3802, 2a2-3604, 2a2-3208, 2a2-2713 and s2020 for the  
 151 two-against-two systems and are 1a3-0525, 1a3-1123, s2020, 1a3-3515, 1a3-5010 and 1a3-6505 for  
 152 the one-against-three systems.

153

154 The polymers were dispersed in a simulation box, for which periodic boundary conditions were  
 155 employed. The number of molecules was 200, both for A and B polymers to attain equimolar  
 156 conditions. The bead number density was fixed at 4. This density is sufficiently higher than the  
 157 overlapping concentration<sup>30</sup> of prepolymers ( $C^* \sim 0.8$ ), and we did not observe any structural  
 158 inhomogeneity even after the gelation. Figure 2 shows a typical snapshot of an s2020 system. Note  
 159 that all the chains are phantom, and bead overlapping is allowed. For sols, equilibration was attained  
 160 with  $f_{ik} = 1$  and the numerical integration time step size  $\Delta t = 0.1$ . The equilibration time was  
 161 chosen at  $10^4$ , which is sufficiently longer than the Rouse relaxation time of prepolymers ( $< 300$ ).

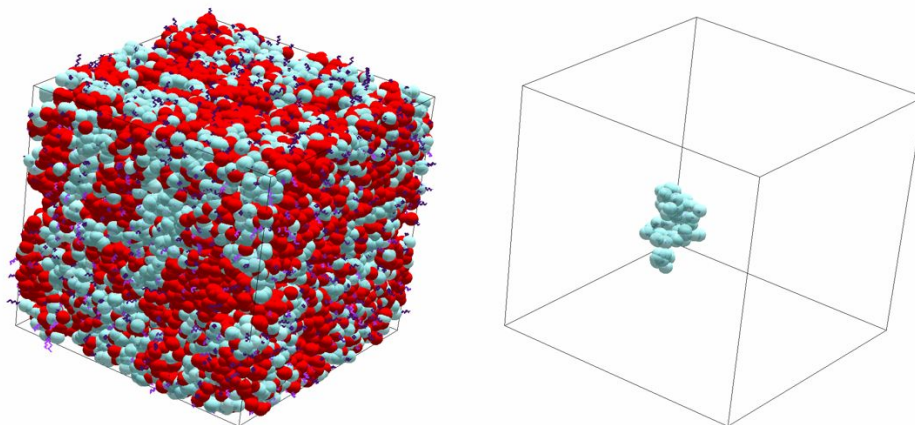
162

163 After equilibration of sols, we performed gelation simulations with  $f_{ik} = 1$  and  $\Delta t = 0.1$ . We had  
 164 a reaction site at the end of each arm stemming from the branch point. This reaction site was  
 165 connected to another one when the two reaction sites came close within a predetermined reaction  
 166 distance with a certain reaction probability and only when the subjected two sites were on the  
 167 different types of molecules. We chose the reaction distance at unity and the cumulative probability  
 168 at 0.1, respectively. The gelation was performed until the conversion ratio became more than 99% as  
 169 shown later.

170

171 The mechanical properties of created networks were examined as follows. To see the elastic  
 172 modulus, we uniaxially stretched the network with  $f_{ik} = 1$  and  $\Delta t = 0.1$ . The stretch rate was  $\dot{\epsilon}$   
 173  $= 2 \times 10^{-5}$ , which is sufficiently lower than the relaxation rate of the single strand. We also  
 174 performed stretch simulations considering bond scission to discuss the toughness of networks. In this  
 175 case, we employed the non-linear spring with finite extensibility to avoid bond scission due to  
 176 thermal fluctuations. (One may argue that such a thermal degradation does not occur if the critical  
 177 bond length of scission is set at a large value. However, in such a case, we have to apply an  
 178 impractical magnitude of stretch to achieve the scission.) The length of each bond was monitored,  
 179 and the bond was broken when  $|\mathbf{b}_{ij}| > 0.9b_{\max}$  (with  $b_{\max} = 3$  as mentioned above). The result of  
 180 the fracture simulation strongly depends on the stretch rate, as shown in Supporting Information,  
 181 because of large-scale structural relaxations following every single bond scission. We empirically  
 182 chose the stretch rate at  $\dot{\epsilon} = 2 \times 10^{-5}$ , below which the result is practically insensitive to the stretch  
 183 rate.  $\Delta t$  for the breakage simulations was chosen at 0.002 according to the tests reported in  
 184 Supporting Information.

185



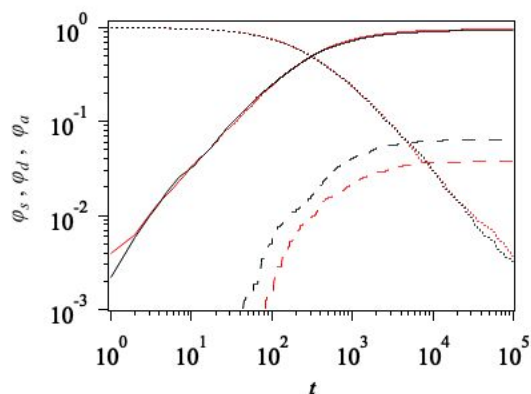
186

187 **Figure 2** Snapshot of an equilibrated sol for the s2020 system and one of the involved 800  
 188 molecules. Red and blue beads represent the segments on type-A and B prepolymers, respectively.

189

190 **3. RESULTS AND DISCUSSION**191 **3.1 Gelation Kinetics and Network Structures**

192 Figure 3 shows the time development of the arm number fractions for different connectivity for  
 193 2a2-3802 and s2020.  $\varphi_a$  is the fraction of unreacted arms. Because all the arms are unreacted at  
 194  $t = 0$ ,  $\varphi_a$  decays from unity. In the long-time region,  $\varphi_a$  exhibits a power-law decay with the  
 195 exponent of -1. This behavior is consistent with the mean-field theory<sup>31,32</sup>. In most experimental  
 196 studies, the exponent is larger than -1 due to the retardation induced by several reasons, including  
 197 entanglement between polymers<sup>33,34</sup>. We do not consider such effects for simplicity. In the resultant  
 198 network at  $t = 10^5$ , the conversion rate is more than 99%. The entire behavior of  $\varphi_a$  is not  
 199 sensitive to all the examined prepolymers regardless of the arm length contrast. This result is rational  
 200 in the late stage because the molecular weight is common, and the diffusion constant of the  
 201 prepolymers is identical.  $\varphi_s$  and  $\varphi_d$  are the fractions of reacted arms forming the single and  
 202 double linkages. Here, a single linkage means that two network nodes are connected only by a single  
 203 network strand. As mentioned above, a double linkage is referred to as a cyclic loop or a secondary  
 204 loop in earlier studies.<sup>30</sup>  $\varphi_d$  is apparently larger for the case with the arm length contrast 2a2-3802  
 205 (black broken curve) than that for the symmetric arm length s2020 (red broken curve). Due to this  
 206 difference, the number of single links (solid curves) depends on the arm length contrast, though it is  
 207 not visible in the log plot. We do not discuss triple and quad linkages<sup>27</sup> because the fraction is quite  
 208 small.



209

210 **Figure 3** Time development of number fraction of the arms. Dotted, solid, and broken curves are  
 211 unreacted dangling ones  $\varphi_a$ , the fraction involved in single linkages  $\varphi_s$ , and those contributed as  
 212 double linkages  $\varphi_d$ , respectively. Black and red curves are for 2a2-3802 and s2020, respectively.

213

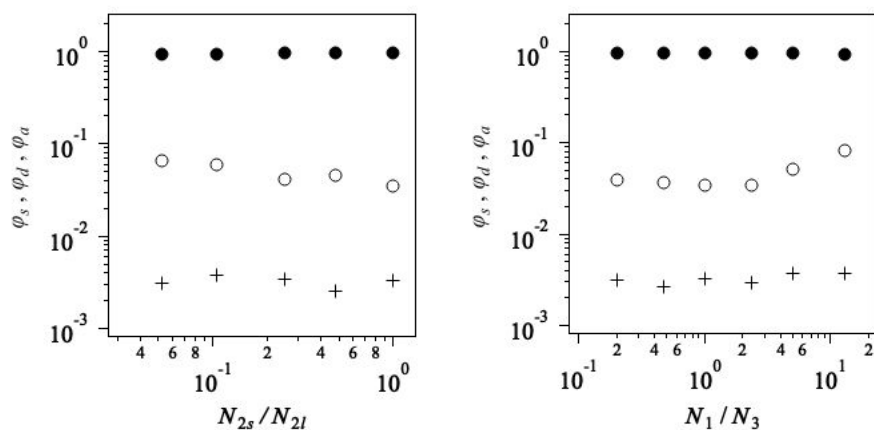
214 Figure 4 shows  $\varphi_a$ ,  $\varphi_s$ , and  $\varphi_d$  in the resultant network plotted against the arm length contrast.  
 215 Hereafter,  $N_{2s}/N_{2l}$  is the bead number ratio of the short arms to the long arms for 2a2 systems, and  
 216  $N_1/N_3$  is that of the minor arms to the major arms for 1a3 systems. As seen in Fig 4, most of the



217 strands form single linkages, and the arm fraction involved in such strands,  $\varphi_s$ , is close to unity for  
 218 all the examined cases (see filled circle). The fraction of unreacted arms,  $\varphi_a$ , is independent of the  
 219 arm length contrast and less than 0.4% (see cross). In contrast, the arm fraction in double linkages  
 220  $\varphi_d$  (unfilled circle) depends on the arm length contrast. Both panels exhibit that the double link  
 221 formation is enhanced when the contrast becomes large.

222

223 For the symmetric case ( $N_{2s}/N_{2l} = N_1/N_3 = 1$ ), Lange et al.<sup>22</sup> have reported  $\varphi_d$  as a function of  
 224 the prepolymer concentration  $C$  normalized by the overlapping concentration  $C^*$ . According to  
 225 their Monte Carlo simulations, the value of  $\varphi_d$  at our concentration ( $C/C^* \sim 5$ ) is ca. 0.05. This  
 226 value is close to but slightly larger than our result ( $\varphi_d = 0.04$ ). The discrepancy is probably due to  
 227 the excluded volume effect neglected in our simulations and the difference in the employed models  
 228 for the reaction kinetics. The other simulations<sup>23,27</sup> suggest similar values of  $\varphi_d$ , though a direct  
 229 comparison is difficult.



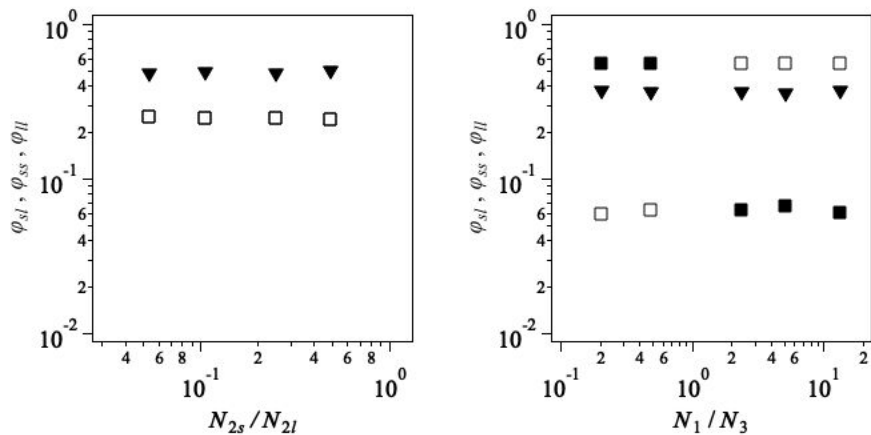
230

231 **Figure 4** Arm fractions in dangling ends  $\varphi_a$  (cross), single linkages  $\varphi_s$  (filled circle), and double  
 232 linkages  $\varphi_d$  (unfilled circle) in the resultant networks for 2a2 and 1a3 systems.

233

234 Figure 5 shows the number fraction of strands formed by two short arms  $\varphi_{ss}$ , long arms , and long  
 235 and short arms  $\varphi_{sl}$ . For 2a2 systems (left panel),  $\varphi_{sl} \sim 1/2$  (triangle) and  $\varphi_{ss} \sim \varphi_{ll} \sim 1/4$  (square).  
 236 For 1a3 systems (right panel),  $\varphi_{ll}$  and  $\varphi_{ss}$  are  $1/16$  or  $9/16$  (filled and unfilled square),  
 237 depending on which arm is dominant.  $\varphi_{sl} \sim 6/16$  (triangle). These results are consistent with the  
 238 expected values from the number ratio between short and long arms. The effect of the unreacted  
 239 portion is negligible.

240



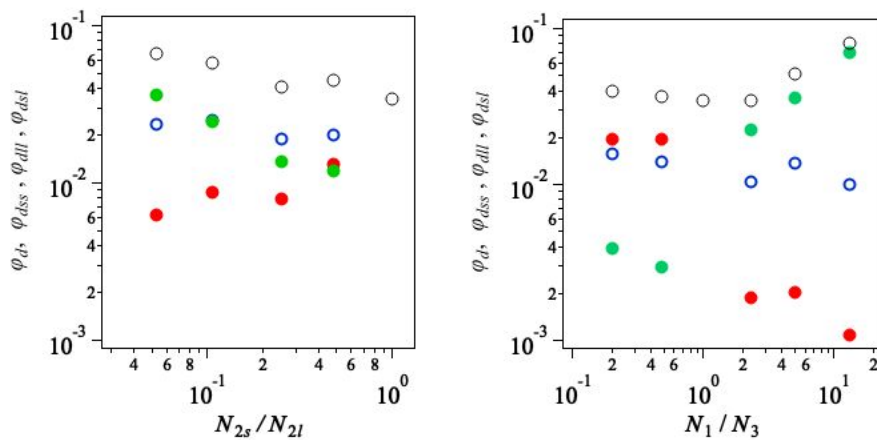
241

242 **Figure 5** Strand fractions formed with two short arms  $\varphi_{ss}$  (unfilled square), two long arms  $\varphi_{ll}$   
 243 (filled square), and short and long arms (triangle)  $\varphi_{sl}$  for 2a2 and 1a3 systems. For 2a2 systems,  
 244  $\varphi_{ll}$  and  $\varphi_{ss}$  overlap with each other; thus,  $\varphi_{ll}$  is not visible.

245

246 Figure 6 shows the fractions of double linkages formed by two short arms  $\varphi_{dss}$ , two long arms  $\varphi_{dll}$ ,  
 247 and a pair of short and long arms  $\varphi_{dsl}$ .  $\varphi_d (= \varphi_{dss} + \varphi_{dll} + \varphi_{dsl})$  is also plotted for comparison.  
 248 Note that  $\varphi_d$  cannot be decomposed for the symmetric case ( $N_{2s}/N_{2l} = N_1/N_3 = 1$ ). For 2a2  
 249 systems (left panel),  $\varphi_{dss}$  (green filled circle) is dominant when  $N_{2s}/N_{2l}$  is small. With increasing  
 250  $N_{2s}/N_{2l}$ ,  $\varphi_{dss}$  decreases and becomes smaller than  $\varphi_{dsl}$  (blue unfilled circle). In contrast,  $\varphi_{dll}$   
 251 (red filled circle) increases with increasing  $N_{2s}/N_{2l}$ . For 1a3 systems (right panel), due to the  
 252 asymmetry of the arm number,  $\varphi_{dll}$  is much larger than  $\varphi_{dss}$  when  $N_1/N_3 < 1$ . In contrast,  
 253 double linkages for  $N_1/N_3 > 1$  are formed mainly by the short-short connection, and  $\varphi_{dll}$   
 254 becomes negligible.  $\varphi_{dsl}$  is not that sensitive to the arm length contrast for both cases.

255



256

257 **Figure 6** Strand fractions in double linkages formed by the arm combinations of short-short  $\varphi_{dss}$   
 258 (green filled circle), long-long  $\varphi_{dll}$  (red filled circle), and short-long  $\varphi_{dsl}$  (blue unfilled circle).

259 The total fraction of double linkages  $\varphi_d$  (unfilled black circle) is also shown for comparison. Note  
 260 that for the monodisperse case (s2020, for which  $N_{2s}/N_{2l} = N_1/N_3 = 1$ ), the strand length is  
 261 uniform, and  $\varphi_d$  cannot be decomposed.

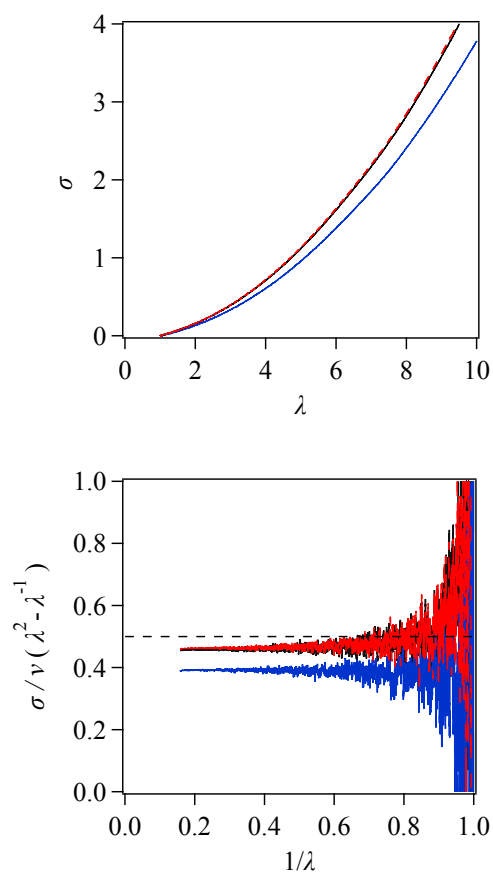
262

### 263 **3.2 Elastic modulus of Gaussian Networks**

264 To evaluate the fraction of effective strands that contribute to the mechanical response, we stretched  
 265 the networks with  $f_{ik} = 1$ . Figure 7 shows the stress-stretch ( $\sigma - \lambda$ ) relation and the Mooney plot.  
 266 In the latter, we normalize the stress by  $\nu(\lambda^2 - \lambda^{-1})$  (where  $\nu$  is the strand number density  
 267 calculated from the number of prepolymers) and plot it against  $\lambda^{-1}$  to see if the ( $\sigma - \lambda$ ) relation  
 268 follows the neo-Hookean prediction. As seen for the large  $\lambda$  region (i.e., the small  $\lambda^{-1}$  region), the  
 269 normalized stress exhibits a horizontal line consistent with the neo-Hookean behavior. We note that  
 270 the stress fluctuations are large in the small  $\lambda$  region even though the presented results are  
 271 ensemble-averaged for eight different networks, and the fluctuations are not visible in the top panel.

272

273 Nevertheless, assuming the neo-Hookean behavior, we can determine the elastic modulus  $G = \sigma/\nu(\lambda^2 - \lambda^{-1})$   
 274 by averaging the value in the range  $\lambda^{-1} \leq 0.5$ , where the  $\lambda$ -independent behavior is  
 275 clearly seen in Fig 7. The value of  $G$  is slightly smaller than the theoretical value of 0.5 for the  
 276 defect-free network<sup>35,36</sup>. As discussed earlier<sup>22,24,27</sup>, this reduction of  $G$  is due to defects that do not  
 277 sustain the stress. (Note that the strand number density  $\nu$  introduced above is calculated from the  
 278 number of dispersed prepolymers, and inactive strands and double linkages are not excluded.) As we  
 279 see that the modulus of the symmetric case (s2020, red curve) and that of a 2a2 system (2a2-3802,  
 280 black curve) are similar, the fraction of defects is not drastically affected by the arm length contrast.  
 281 Meanwhile, the randomly connected network (Rnd, blue curve) exhibits a modulus significantly  
 282 smaller than the tetra-branched networks.



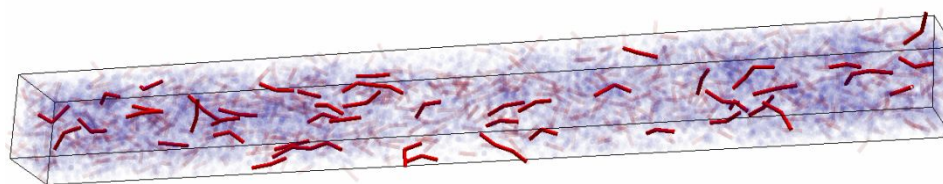
283

284 **Figure 7** Stress-strain relation under uniaxial stretch with a constant stretch rate for s2020 (red  
 285 broken), 2a2-3802 (black solid), and Rnd (blue solid). The broken horizontal line indicates the value  
 286 of 0.5.

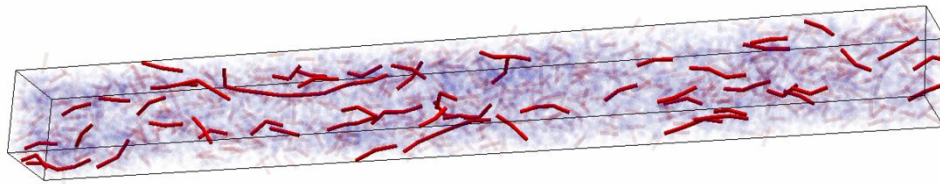
287

288 Figure 8 top panel shows the spatial distribution of stretched segments for a s2020 network at the  
 289 applied stretch of 5. This snapshot exhibits no clear force chain formation<sup>37</sup>, implying that the stress  
 290 is not localized. Although not shown, the distribution for the other tetra systems is similar even for  
 291 the systems formed by highly asymmetric prepolymers. In contrast, in the bottom panel for Rnd,  
 292 there exist some long, colored chains that indicate stress localization along the dominant force  
 293 chains. This result is consistent with the modulus shown in Fig 7.

294



295



296

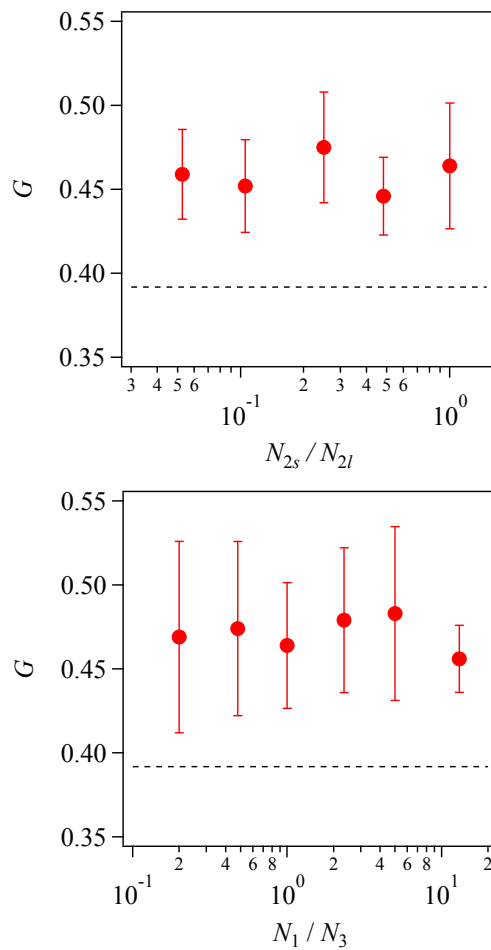
297

298 **Figure 8** Distribution of stretched segments (red cylinders) in resultant gels for s2020 (top) and Rnd  
299 (bottom) under the applied stretch  $\lambda = 5$ . The stretched segments are highlighted when consecutive  
300 segments are stretched. For the colored segments, the squared segment length is larger than 3. The  
301 dispersed beads are also shown by light blue spheres.

302

303 Figure 9 shows the modulus  $G$  as functions of the arm length contrast for 2a2 and 1a3 systems. As  
304 the difference is within the error-bar, the modulus is essentially insensitive to the arm length  
305 contrast. Since the modulus is more than 0.45, 90% of the strands carry the stress for the examined  
306 tetra-branched networks. Meanwhile, the modulus is ca 0.38 for Rnd, indicating that the fraction of  
307 effective strands is less than 80%. Since Rnd systems were created from single chains, there are  
308 neither isolated clusters nor dangling ends. As such, the small modulus reflects inhomogeneity due  
309 to the widely dispersed strand length. In this respect, modulus of tetra-branched networks would  
310 become lower if further contrast is introduced for the strand length.

311



312

313 **Figure 9** Modulus plotted against the arm length contrast for 2a2 (top) and 1a3 (bottom) systems.  
 314 The horizontal broken line indicates the value for Rnd. The error bar shows the standard deviation  
 315 among 8 different systems for s2020.

316

### 317 3.3 Fracture

318 Figure 10 shows stress-stretch relations for 2a2 systems with bond scission. (The results for 1a3  
 319 systems are available in Supporting Information.) The stress  $\sigma$  grows up to a certain maximum  
 320  $\sigma_{\max}$ , it decays following the peak. The stretch at the peak  $\lambda_p$  is located around 16 for s2020. This  
 321  $\lambda_p$  is consistent with the maximum stretch  $\lambda_{\max}$  for a single network strand containing 40 bonds  
 322 with the maximum bond stretch of 3 ( $\lambda_{\max} = 3 \times 40/\sqrt{40} \sim 19$ ). The curves for 8 independent  
 323 simulation runs are rather similar to each other for s2020, whereas the curves become diverse for the  
 324 networks with asymmetrical strand lengths. For instance, the curves largely scatter for the random  
 325 networks (Rnd) to exhibit similar  $\sigma_{\max}$  and different mitigation behaviors. This variation of  $\lambda_p$   
 326 implies that the bond scission happens at network strands with various segment numbers. Indeed, for  
 327 the tetra-networks with asymmetrical strand lengths, we see a few bundles of curves that reflect the

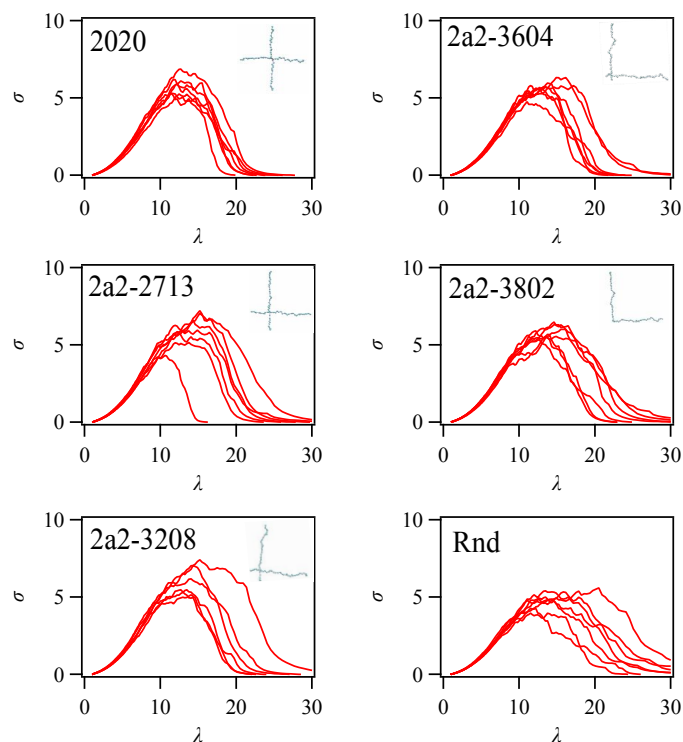
328 strand length subjected to the scission. Takahashi et al.<sup>19</sup> have shown that for PDMS gels the  
329 elongation at break is significantly reduced when they introduced the strand length distribution. Our  
330 result is in harmony with this report, though a direct comparison is difficult since our polydispersity  
331 index is only 2 for Rnd, whereas it was ca. 600 for their study.

332

333 We note that the simulated stress-strain curves are different from typical experimental data. Namely,  
334 in most of mechanical experiments, the stress immediately drops to zero when the specimen is  
335 broken, and the stress exhibits a sharp-edged peak. In contrast, the simulated stress mitigates with a  
336 certain duration after a dull peak. This discrepancy is due to structural relaxations induced by every  
337 single bond scission. The structural relaxation takes place with a long relaxation time, when the  
338 fragmented dangling domains become large. If we choose a stretch rate smaller than the slowest  
339 relaxation rate of the entire system, it should be smaller than  $\dot{\epsilon} = 3 \times 10^{-8}$  as we have 32,800  
340 Rouse beads in total. Such a stretch rate is significantly smaller than the employed rate chosen at  $\dot{\epsilon}$   
341  $= 2 \times 10^{-5}$ , being hardly achieved with practical computation costs. One may argue that this  
342 problem can be solved if the network structure is immediately relaxed at each bond scission  
343 according to the energy minimization<sup>25,38</sup>. For example, Lei et al.<sup>38</sup> have reported such a calculation,  
344 in which obtained stress-strain relations are close to typical experiments. However, they neglect  
345 thermal fluctuations at the network nodes, and thus, the model construction is rather macroscopic.  
346 Arora et al.<sup>28</sup> have very recently reported another simulation scheme to discuss the effect of primary  
347 loops on the mechanical properties of the network. Although they cleverly implemented relaxation  
348 process during the network fracture in their numerical scheme, their stress-strain curves are similar  
349 to ours with exhibiting dull peaks. As such, at the best of our knowledge, no impeccable simulation  
350 scheme for the targeted problem is available at the present. Nevertheless, we have confirmed that the  
351 result does not strongly depend on the stretch rate below the employed value as shown in Supporting  
352 Information, and we note that the presented results include the effect of structural relaxations.

353

354



355

356 **Figure 10** Stress-stretch curves for 2a2 systems. The results from 8 independent simulation runs are  
 357 shown. The results for the random network (Rnd) are also shown for comparison. The results for 1a3  
 358 systems are available in Supporting Information.

359

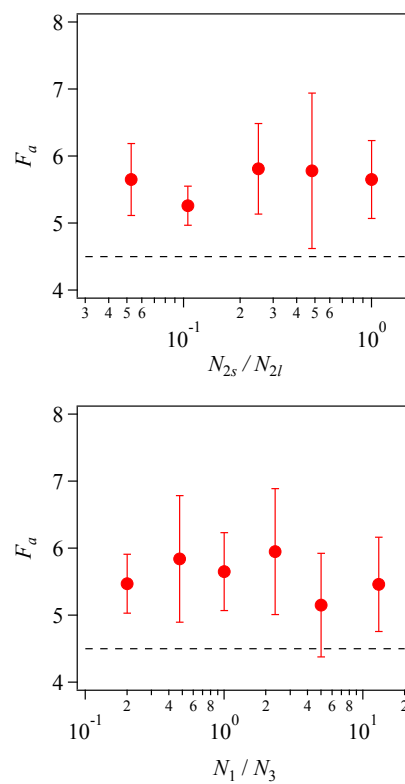
360 We evaluated the toughness from the obtained stress-strain curves by numerically integrating the  
 361 curve to obtain the required work for fracture. (Note that the curves in Fig 10 exhibit true stress  
 362 versus stretch, and the work for fracture was calculated from the relation between true stress versus  
 363 true strain.) Figure 8 shows the apparent fracture energy  $F_a$ , which is the required work for the  
 364 network fracture calculated from the stress-strain curve. Note that we refer to  $F_a$  as the apparent  
 365 energy because the stress-stretch curve includes the contribution of structural relaxation as  
 366 mentioned above. The examined tetra-networks exhibit higher  $F_a$  values than the random network  
 367 (shown by broken horizontal line) being essentially independent of the arm length contrast of  
 368 prepolymers. This result is in harmony with the experiment by Sakai et al.<sup>16</sup>

369

370 One may argue that our result is different from earlier studies for end linked PDMS gels, for which  
 371 the toughness is significantly dependent on the bimodality of the network strand<sup>18,39-42</sup>. The  
 372 discrepancy is highly probably due to the difference in the short strand fraction. The basic strategy  
 373 proposed by Mark<sup>39</sup> for the improvement of mechanical properties is the inclusion of a small number  
 374 of long strands in a network mainly composed of short prepolymers. For example, in the case of  
 375 Llorente et al.<sup>40</sup>, the fraction of short strand is 90% for the network that exhibits a superior



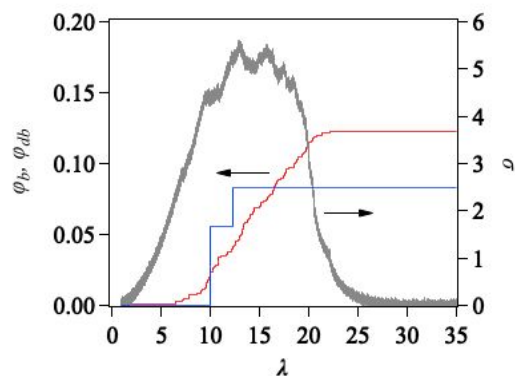
376 mechanical property. Our examined cases for the 2a2 networks are opposite; long strands are the  
 377 majority. For the 1a3 systems, the network strands are trimodal (see Supporting Information).  
 378 Nevertheless, the volume fraction of the shortest strand is not the largest. The strand length contrast  
 379 is also different from each other. For the study by Llorente et al.<sup>40</sup>, the molecular weights of  
 380 prepolymers are 660 and 220g/mol for the short chains and 18500g/mol for the long chain. The  
 381 ratios of the short strand lengths to that of the long chain are 0.035 and 0.012, respectively. These  
 382 ratios are smaller than our smallest ratio  $4/76 = 0.053$  realized for 2a2-3802.  
 383  
 384



385  
 386 **Figure 11** Apparent fracture energy obtained from the stress-stretch curves plotted against the arm  
 387 length ratio for 2a2 (top) and 1a3 (bottom) systems. Horizontal broken lines indicate the value for  
 388 Rnd. Error bars correspond to the standard deviation for 8 independent simulation runs.

389  
 390 Figures 4 and 11 demonstrate that the inclusion of double linkages does not improve the toughness  
 391 of tetra-networks. We rationalize this result by exhibiting the scission rate of linkages. Figure 12  
 392 shows a typical example of the fraction of broken strands during the stretch for one of the 1a3-6505  
 393 networks. The stress and the broken fraction of double linkages are also shown for comparison. The  
 394 network does not sustain stress after the broken strand fraction reaches ca.  $\varphi_b \sim 0.13$ . Meanwhile, for  
 395 this specific case, we observe the scission of double linkages up to  $\varphi_{db} = 0.08$ . Note that  $\varphi_{db}$  is the

396 ratio of broken double linkages to all the embedded double linkages. Because the number of double  
 397 linkages is not large as shown in Fig 4, the evolution of  $\varphi_{db}$  is discrete.



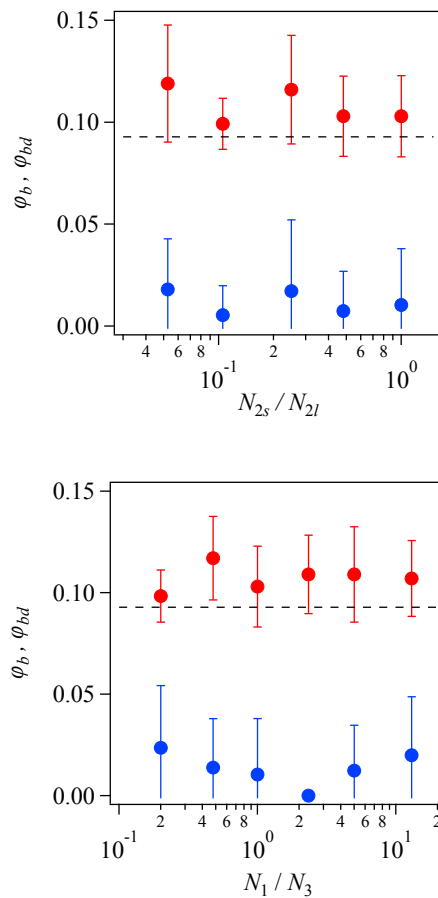
398

399 **Figure 12** Evolution of the broken strand fraction  $\varphi_b$  (red curve) during stretch for a 1a3-6505  
 400 network. Blue line indicates the broken double linkage fraction  $\varphi_{db}$ . Gray curve shows the stress for  
 401 comparison.

402

403 Figure 13 shows the broken strand fraction  $\varphi_b$  and  $\varphi_{db}$  observed at the final broken networks. For  
 404 all the examined tetra-networks,  $\varphi_b$  is ca. 0.12, irrespective of the arm length contrast. This value  
 405 is larger than that for Rnd, originating the toughness shown in Fig 8. Concerning double linkages,  
 406 the broken fraction  $\varphi_{db}$  is less than 1/4 of  $\varphi_b$  for the examined cases. This result demonstrates that  
 407 double linkages are relatively tougher than single linkages. In this respect, our results are in harmony  
 408 with the theory by Lin and Zhao<sup>20</sup>. However, double linkages survive, and they do not contribute to  
 409 toughness of the network, since the fracture propagates mainly through single linkages.  
 410 Consequently, the inclusion of double linkages does not improve the mechanical properties of the  
 411 examined tetra-networks.

412



413

414

415

416

417

418

419

**Figure 13** Broken strand fraction in the final fractured networks  $\varphi_b$  (red) and the fraction of broken double linkages to all the embedded double linkages  $\varphi_{db}$  (blue) against the arm length ratio for 2a2 (top) and 1a3 (bottom) systems. Horizontal broken lines indicate the value for Rnd. Error bars correspond to the standard deviation for 8 independent simulation runs.

#### 4 CONCLUSIONS

420

421

422

423

424

425

426

427

428

429

430

To discuss the effect of arm length distribution of prepolymers for tetra gels, we performed Brownian simulations for a series of tetra prepolymer mixtures with various bidispersed prepolymer arm lengths, without considering the solvent explicitly. Since we did not consider the excluded volume effect, the gelation kinetics followed the mean-field theory, and the conversion ratio was more than 99% for all the examined cases. For the resultant networks, number of ineffective strands involved in dangling and isolated clusters was estimated from the elastic modulus. The obtained modulus indicated that more than 90% of the strands contributed to the stress, irrespective of the arm length contrast of prepolymers. Besides, we observed the formation of double linkages, and their number increased with increasing the arm molecular weight contrast. To the resultant networks, we applied large stretch to observe the network fracture by introducing bond scission. From the observed stress-stretch curves, we calculated the apparent work for fracture to discuss the toughness

431 of networks. The obtained fracture energy does not depend on the arm length contrast of  
432 prepolymers. This insensitivity of toughness to the strand length distribution is in harmony with the  
433 earlier experimental study<sup>16</sup>. The result also implies that the toughness is not sensitive to the  
434 inclusion of double linkages, contrary to the recent theoretical prediction<sup>20</sup>. This inconsistency is  
435 indeed due to the toughness of double linkages, which are rarely broken in comparison to single  
436 linkages. As such, to be fair, we note that the double linkages may improve network toughness as  
437 theoretically suggested, if the fraction of double linkages becomes higher than the examined range,  
438 and/or the double linkages are installed to the network by different strategies from the present work.

439

440 Concerning the employed model and the simulation scheme, the present results include some effects  
441 of network relaxation during the fracture. Besides, we did not consider non-bonded interactions and  
442 solvent molecules, which may change the results via the effects of entanglement and network  
443 swelling. For a quantitative comparison to a specific experiment, a coarse-grained model  
444 systematically constructed as proposed earlier<sup>26</sup> is necessary. Studies toward such directions are  
445 ongoing and the results will be reported elsewhere.

446

#### 447 **Acknowledgement**

448 This study was supported in part by JST-CREST (JPMJCR1992), and JSPS KAKENHI Grant  
449 Number 22H01189.

450

#### 451 **REFERENCES**

- 452 1 M. Shibayama, X. Li and T. Sakai, *Colloid and Polymer Science*, 2019, **297**, 1–12.
- 453 2 T. Sakai, *Nihon Reoroji Gakkaishi*, 2019, **47**, 183–195.
- 454 3 D. G. Wallace, G. M. Cruise, W. M. Rhee, J. A. Schroeder, J. J. Prior, J. Ju, M. Maroney, J.  
455 Duronio, M. H. Ngo, T. Estridge and G. C. Coker, *Journal of Biomedical Materials Research*,  
456 2001, **58**, 545–555.
- 457 4 T. Sakai, T. Matsunaga, Y. Yamamoto, C. Ito, R. Yoshida, S. Suzuki, N. Sasaki, M. Shibayama  
458 and U. Chung, *Macromolecules*, 2008, **41**, 5379–5384.
- 459 5 K. Nishi, K. Fujii, Y. Katsumoto, T. Sakai and M. Shibayama, *Macromolecules*, 2014, **47**, 3274–  
460 3281.
- 461 6 K. Hashimoto, K. Fujii, K. Nishi, T. Sakai and M. Shibayama, *Macromolecules*, 2016, **49**, 344–  
462 352.
- 463 7 Y. Yoshikawa, N. Sakumichi, U. Chung and T. Sakai, *Soft Matter*, 2019, **15**, 5017–5025.
- 464 8 T. Katashima, H. Sakurai, U. Chung and T. Sakai, *Nihon Reoroji Gakkaishi*, 2019, **47**, 61–66.
- 465 9 Y. Yoshikawa, N. Sakumichi, U. Chung and T. Sakai, *Physical Review X*, 2021, **11**, 11045.
- 466 10 N. Sakumichi, Y. Yoshikawa and T. Sakai, *Polymer Journal*, 2021, **53**, 1293–1303.

- 467 11 D. E. Apostolides, C. S. Patrickios, T. Sakai, M. Guerre, G. Lopez, B. Améduri, V. Ladmiral, M.  
468 Simon, M. Gradzielski, D. Clemens, C. Krumm, J. C. Tiller, B. Ernould and J. F. Gohy,  
469 *Macromolecules*, 2018, **51**, 2476–2488.
- 470 12 T. Fujiyabu, N. Sakumichi, T. Katashima, C. Liu, K. Mayumi, U. Chung and T. Sakai, *Science*  
471 *Advances*, 2022, **8**, 1–10.
- 472 13 S. Okata, K. Hoshina, K. Hanada, H. Kamata, A. Fujisawa, Y. Yoshikawa and T. Sakai, *Annals of*  
473 *Vascular Surgery*, 2022, 1–7.
- 474 14 Y. Miura, Y. Tsuji, R. Cho, A. Fujisawa, M. Fujisawa, H. Kamata, Y. Yoshikawa, N. Yamamichi,  
475 T. Sakai and K. Koike, *Scientific Reports*, 2021, **11**, 1–7.
- 476 15 K. Hayashi, F. Okamoto, S. Hoshi, T. Katashima, D. C. Zujur, X. Li, M. Shibayama, E. P. Gilbert,  
477 U. Chung, S. Ohba, T. Oshika and T. Sakai, *Nature Biomedical Engineering*, 2017, **1**, 1–7.
- 478 16 T. Sakai, Y. Akagi, S. Kondo and U. Chung, *Soft Matter*, 2014, **10**, 6658–6665.
- 479 17 A. L. Andrady, M. A. Llorente and J. E. Mark, *The Journal of Chemical Physics*, 1980, **72**, 2282–  
480 2290.
- 481 18 Z. Zhang and J. E. Mark, *Journal of Polymer Science: Polymer Physics Edition*, 1982, **20**, 473–  
482 480.
- 483 19 H. Takahashi, Y. Ishimuro and H. Watanabe, *Polymer Journal*, 2008, **40**, 465–474.
- 484 20 S. Lin and X. Zhao, *Physical Review E*, 2020, **102**, 52503.
- 485 21 P. G. de Gennes, *Scaling concepts in polymer physics*, Cornell University Press, Ithaca, 1979.
- 486 22 F. Lange, K. Schwenke, M. Kurakazu, Y. Akagi, U. Chung, M. Lang, J. U. Sommer, T. Sakai and  
487 K. Saalwächter, *Macromolecules*, 2011, **44**, 9666–9674.
- 488 23 T. S. Lin, R. Wang, J. A. Johnson and B. D. Olsen, *Macromolecules*, 2018, **51**, 1224–1231.
- 489 24 K. Nishi, H. Noguchi, T. Sakai and M. Shibayama, *The Journal of Chemical Physics*, 2015, **143**,  
490 184905.
- 491 25 A. Sugimura, M. Asai, T. Matsunaga, Y. Akagi, T. Sakai, H. Noguchi and M. Shibayama,  
492 *Polymer Journal*, 2013, **45**, 300–306.
- 493 26 E. Wang and F. Escobedo, *Macromolecular Theory and Simulations*, 2017, **26**, 1–12.
- 494 27 T. Furuya and T. Koga, *Polymer*, 2020, **189**, 122195.
- 495 28 A. Arora, T. S. Lin and B. D. Olsen, *Macromolecules*, 2022, **55**, 4–14.
- 496 29 R. L. Honeycutt, *Physical Review A*, 1992, **45**, 600–603.
- 497 30 T. Sakai, *Physics of Polymer Gels*, Wiley, 2020.
- 498 31 D. Toussaint and F. Wilczek, *The Journal of Chemical Physics*, 1983, **78**, 2642–2647.
- 499 32 K. Kang and S. Redner, *Physical Review A*, 1985, **32**, 435–447.
- 500 33 D. S. Achilias, *Macromolecular Theory and Simulations*, 2007, **16**, 319–347.
- 501 34 Y. Masubuchi and T. Uneyama, *Soft Matter*, 2019, **15**, 5109–5115.
- 502 35 P. J. Flory, *Proceedings of the Royal Society of London. A. Mathematical and Physical Sciences*,

- 503 1976, **351**, 351–380.
- 504 36 R. Everaers, *New Journal of Physics*, 1999, **1**, 12.1-12.54.
- 505 37 R. Everaers, K. Kremer and G. S. Grest, *Macromolecular Symposia*, 1995, **93**, 53–67.
- 506 38 J. Lei, Z. Li, S. Xu and Z. Liu, *Journal of the Mechanics and Physics of Solids*, 2021, **156**,  
507 104599.
- 508 39 J. E. Mark, *Rubber Chemistry and Technology*, 1999, **72**, 465.
- 509 40 M. A. Llorente, A. L. Andradý and J. E. Mark, *Journal of Polymer Science: Polymer Physics*  
510 *Edition*, 1981, **19**, 621–630.
- 511 41 J. E. Mark and M. Y. Tang, *Journal of polymer science. Part A-2, Polymer physics*, 1984, **22**,  
512 1849–1855.
- 513 42 J. E. Mark, *The Journal of Physical Chemistry B*, 2003, **107**, 903–913.
- 514
- 515